Macromolecules

pubs.acs.org/Macromolecules Article

Mechanisms Controlling the Energy Barrier for Ion Hopping in Polymer Electrolytes

Catalin Gainaru,* Rajeev Kumar, Ivan Popov, Md Anisur Rahman, Michelle Lehmann, Eric Stacy, Vera Bocharova, Bobby G. Sumpter, Tomonori Saito, Kenneth S. Schweizer, and Alexei P. Sokolov*

Cite This: *Macromolecules* 2023, 56, 6051−6059 Read Online

ACCESS | Metrics & More | Article Recommendations | Supporting Information

ABSTRACT: The present work studies the mechanisms controlling the energy barrier for ion hopping in conducting polymers. Polymer electrolytes usually show Arrhenius-like temperature dependence of the conductivity relaxation time (characteristic time of local ion rearrangements) at temperatures below their glass transition T_g. However, our analysis reveals that the Arrhenius fit of this regime leads to unphysically small prefactors, $\tau_0 \ll 10^{-13}$ s. Imposing a value of 10^{-13} s for this parameter renders the fairly unexpected result that the energy barrier for charge transport in these polymers has strong temperature dependence even below T_g. Our study also reveals significant temperature variations of the dielectric permittivity and the instantaneous shear modulus in the glassy state of these polymers. Using the Anderson and Stuart model, we demonstrate that these variations provide strong justifications for the temperature variation of energy barrier for ion hopping. Most importantly, the proposed approach reveals that the energy barrier controlling ion hopping in polymer electrolytes is significantly (∼30−40%) lower than that estimated using traditional Arrhenius fit. These new insights call for revisions of many earlier results based on apparent Arrhenius fits, and the newly proposed approach can provide more accurate guidance for the design of solid-state electrolytes with enhanced ionic conductivity.

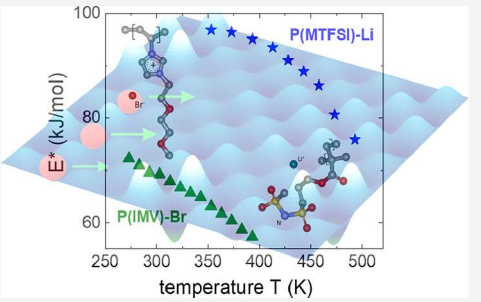

Downloaded via UNIV OF TENNESSEE KNOXVILLE on August 24, 2023 at 23:58:10 (UTC).
See https://pubs.acs.org/sharingguidelines for options on how to legitimately share published articles.

INTRODUCTION

Significant breakthrough in electrical energy storage is expected with the development of solid-state batteries due to their great potential toward high energy density, long cycle life, and safety benefits.[1−4] One of the major bottlenecks in the large-scale deployment of these batteries is the absence of a solid electrolyte with good conductivity, electrochemical stability, mechanical flexibility, and adhesion to electrodes. Polymer electrolytes might provide a good solution due to their flexibility, good adhesion, and easy processability.[5,6] However, the conductivity of dry (with no solvent) polymer electrolytes remains rather low,[7−9] and understanding the detailed microscopic mechanism controlling ion transport in polymers is critical for the development of novel electrolytes.

In classical polymer electrolytes, such as poly(ethylene oxide) (PEO), the lithium ions are coordinated by the backbone ether oxygen atoms; hence, the conductivity is dynamically coupled to the segmental rearrangements of the polymer.[10,11] In this case, reaching desired conductivity levels of 10^{-4}−10^{-3} S/cm requires extremely fast segmental relaxation times ∼10^{-9}−10^{-10} s,[12] not achievable in ambient conditions for dry polymers at high ion concentrations. Additionally, PEO-based electrolytes also suffer from low cation transference number t^+ and a limited electrochemical stability window.[13]

The problem of low t^+ can be solved using single-ion conducting polymers (SICPs), such as polymerized ionic liquids (PolyILs), that have $t^+ \sim 0.8$−1.[14−17] However, SICPs also exhibit relatively low conductivities at ambient conditions.[9,12,18,19] Many of them have conductivity decoupled from segmental dynamics, with characteristic rates of ion transport significantly (∼10^5−10^8 times) faster than that of their segmental motions close to their glass transition temperature T_g.[20,21] In the glassy state of these electrolytes, the ions perform hopping in a dynamically frozen polymer structure, resembling the ion motion in "superionic" ceramics.[22,23] Exhibiting strong degrees of dynamical decoupling and with only one type of charge carrier governing their conductivity, the SICPs are good model systems for the study of ion dynamics in glassy polymers.

Traditionally, the energy barrier E for ionic transport in glassy materials is estimated based on the apparent Arrhenius-like temperature dependence of steady-state conductivity or characteristic conductivity relaxation time:[9,12,18]

$$\tau = \tau_0 \exp(E/RT) \quad (1)$$

Received: May 5, 2023
Revised: June 26, 2023
Published: July 28, 2023

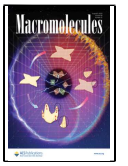

© 2023 American Chemical Society

https://doi.org/10.1021/acs.macromol.3c00879
Macromolecules 2023, 56, 6051−6059

where τ_0 is the prefactor. For the latter, values between 10^{-12} and 10^{-14} s, typical for molecular vibrations and non-activated short time relaxation processes, are usually reported for supercooled liquids,[24,25] polymer melts,[26] and glassy materials.[27] It was argued that a targeted conductivity higher than 10^{-4} S/cm at ambient temperature in the ion hopping regime requires $E \sim 20-30$ kJ/mol.[12] Therefore, understanding the microscopic mechanisms controlling this energy barrier might provide guidance for the design of polymer electrolytes with required conductivity.

About 7 decades ago, Anderson and Stuart (AS) suggested a fairly simple model for describing the energy barriers for ion motions in silicate glasses. The model assumes two major contributions:[28]

$$E(\varepsilon, G_\infty, R_i) \propto \left[\frac{q^2}{4\pi\varepsilon(R_i + R_c)} + G_\infty L(R_i - R_D)^2\right] \quad (2)$$

The first term accounts for the electrostatic attractive interaction, which depends on the material permittivity ε and the radii R_i and R_c of ion and counterion, respectively. The second describes the elastic energy for creating a passage of the size comparable to the cross-section of the mobile ion, which depends on the instantaneous shear modulus G_∞ of the matrix and on the ion jump length L. The additional parameter R_D in eq 2 represents an effective radius of a preexisting doorway and can be considered as a measure of the matrix's "free volume". Note that in this approach the shear modulus corresponds to very high frequencies, far above the rate of ion rearrangements. The idea is that the ion jump itself is very fast (about picosecond time scale), while the waiting time between consecutive jumps (*i.e.*, the relaxation time) can be long. During the jump, the ion "shoves" aside its surroundings, justifying the choice of shear, instead of bulk elastic modulus.[29,30] The AS model describes ionic conductivity in network glasses very well,[25,31] and recently it was demonstrated to work reasonably well also for SICPs in their glassy state.[9,32] These latter studies revealed large values for the activation energy of Li^+ transport in SICPs, of about 150 kJ/mol, far above the 20−30 kJ/mol values required for technical applications.

Here, we present a detailed analysis of the parameters controlling the energy barrier of ion hopping in SICPs. This analysis revealed that the traditional approach (eq 1) for estimating the energy barrier below T_g results in unphysically small Arrhenius prefactors τ_0, below 10^{-20} s. This is in contrast with results for superionic ceramics where the expected $\tau_0 \sim 10^{-12}-10^{-14}$ s holds. We demonstrate that this short τ_0 in SICPs is the consequence of a temperature-dependent activation energy even at $T < T_g$, as predicted theoretically for neat polymer glasses.[33] As a result, the apparent Arrhenius approximation significantly overestimates the energy barrier for ion hopping. Based on these results, we propose a different approach, to estimate the temperature dependence of the effective activation energy $E^*(T)$ and to provide experimental support for the existence of this variation. Guided by the AS model, our analysis revealed that indeed both ε and G_∞ vary significantly with the temperature even below T_g in the studied SICPs and that the temperature variation of these parameters describes well $E^*(T)$. Moreover, the so-estimated energy barriers appear significantly (~30−40%) lower than the ones estimated from the apparent Arrhenius slope.

RESULTS AND DISCUSSION

To analyze details of ion hopping in SICPs, we chose systems with small (Li^+, Na^+), intermediate (Br^-), and large ($TFSI^-$) mobile ions. As discussed below, systematically increasing the size of the free ions is important for tuning the type of interaction between the ions and the matrix. The investigated materials are poly[methacrylate-bis(trifluoromethane)-sulfonimide-lithium] [P(MTFSI)-Li], poly[styrene-bis-(trifluoromethane) sulfonimide-lithium] [P(STFSI)-Li], poly-[methacrylate-bis(trifluoromethane)-sulfonimide-sodium] [P-(MTFSI)-Na], poly[imidazole-vinyl bromide] [P(IMV)-Br], and poly[methacrylate-imidazole-bis(trifluoromethane) sulfonimide] [P(MIM)-TFSI]. These polymers were synthesized at the Oak Ridge National Laboratory (details provided in the Supplemental Material), and their chemical structures are presented in Figure 1. As described there, the samples were carefully dried to remove all traces of solvents prior measurements.

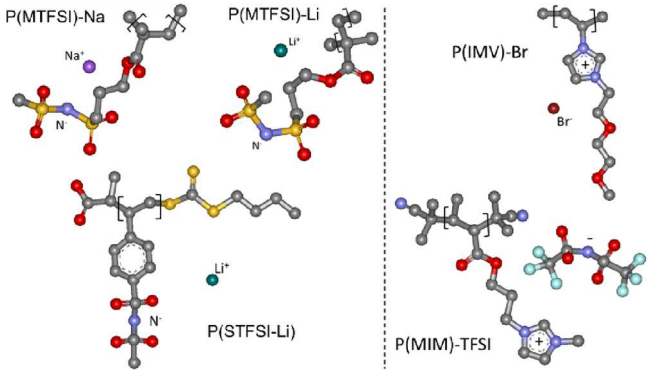

Figure 1. Chemical structure of the investigated single-ion conducting polymers. The dashed line separates materials with mobile cations (left) from those with mobile anions (right). The unlabeled atoms colored with gray, blue, red, orange, and cyan represent carbon, nitrogen, oxygen, sulfur, and fluorine, respectively (hydrogen atoms not shown).

To gain access to glass transition temperatures, time scales of ionic motion, permittivity, and the instantaneous shear modulus of the studied materials, we employed a combination of differential scanning calorimetry, dielectric spectroscopy, and Brillouin light scattering techniques, respectively. Details of the experiments and data analyses are provided in the Methods and Analyses section.

Effective Activation Energy for Charge Transport in Glassy Polymers. The crossover between the AC and DC conductivity regimes identified in the dielectric spectra has been used to estimate the characteristic time of ions crossing from localized, sub-diffusive motion to a regular diffusion[34,35] (see the Methods and Analyses section for details). These conductivity relaxation times τ together with the DC conductivities σ_0 of the investigated materials are presented in Figure 2 as a function of inverse temperature. As observed there, the temperature variations of both τ and σ_0 for P(MTFSI)-Li, P(MTFSI)-Na, P(IMV)-Br and P(MIM)-TFSI change around T_g (Table 1) from a strongly non-Arrhenius, Vogel−Fulcher−Tammann-like behavior, to a weaker, Arrhenius-like form at lower T. This behavior is often observed for ion conductors with strong decoupling between charge transport and structural relaxation.[9,17,18,36]

https://doi.org/10.1021/acs.macromol.3c00879
Macromolecules 2023, 56, 6051−6059

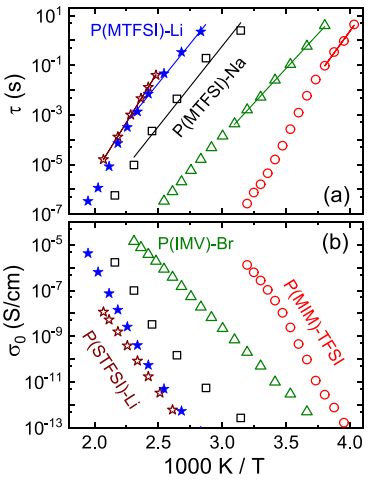

Figure 2. (a) Conductivity characteristic time and (b) DC conductivity as a function of reciprocal temperature for the systems investigated in this work. The solid lines are interpolations of sub-T_g data with eq 1.

Table 1. Glass Transition Temperatures and the Apparent Arrhenius Parameters Extracted with Eq 1 for the Materials Discussed in This Work[a]

material	T_g (K)	logτ_0	E_a (kJ/mol)
P(STFSI)-Li	507	−22	159
P(MTFSI)-Na	433	−19.7	124
P(MTFSI)-Li	435	−17.8	123
P(IMV)-Br	353	−21	107
P(MIM)-TFSI	285	−28	136
polyEtVIm-TFSI[9]	344	−22.4	116
polyEGVIm-TFSI[9]	261	−33	159
PolyEGVIm-Br[9]	348	−18	74
PolyEGVIm-PF6[9]	296	−22.6	118
PolySTF-K[9]	500	−19.7	105
PolySTF-Cs[9]	470	−17.1	87
CKN[40]	333		115
LLTO[36]		−13.1	32.4
Li3B[36]		−14	76.7
YSZ[36]		−15	103

[a]See text for details.

Since P(STFSI)-Li has been investigated only at $T < T_g$, its corresponding parameters exhibit only the Arrhenius-like temperature variations (Figure 2). We note that the values of τ and σ_0 may change at $T \leq T_g$ due to the physical aging of the materials.[37−39] However, in our investigations, the samples have not been aged.

Fits of conductivity relaxation times using eq 1 at temperatures below T_g (Figure 2, solid lines) revealed apparent activation energies E_as comparable to those reported earlier for other SICPs (Table 1).[9,29] Table 1 also includes the fit results for the prefactor τ_0, a parameter which was neglected in previous related studies, including our own.[9,12,17,20,29] These values reveal that for SICPs, in general, τ_0 is unphysically short, with variations around 10^{-20}−10^{-30} s. In contrast, the expected relation $\tau_0 \sim 10^{-12}$−10^{-14} s holds well for crystalline and glassy superionic conductors,[40] as demonstrated for several systems in Table 1 and Figure 3. These results are not entirely unexpected given that glass-forming polymers are "fragile" corresponding to a significant change of structure with

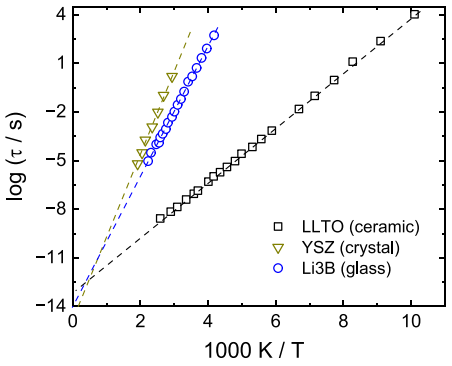

Figure 3. Conductivity characteristic times as a function of reciprocal temperature for ceramic $Li_{0.18}La_{0.61}TiO_3$ (LLTO), crystalline yttria-stabilized zirconia ($ZrO_2{\cdot}Y_2O_3$, YSZ), and $Li_2O{\cdot}3B_2O_3$ (Li3B) glass.[36]

temperature and super-Arrhenius relaxation in the deeply supercooled state, in contrast to ceramics, which are "strong" glasses with little configurational changes of structure and (nearly) Arrhenius relaxation over a wide range of temperatures. Indeed, even in pure polymers below T_g, an apparent Arrhenius behavior is observed for the alpha relaxation time.[41,42] An extrapolation of this behavior to $1/T \rightarrow 0$ often results in an unphysically small prefactor.

To better illustrate the peculiar relaxation behavior of glassy polymers, the data from Figure 2 are presented in Figure 4a

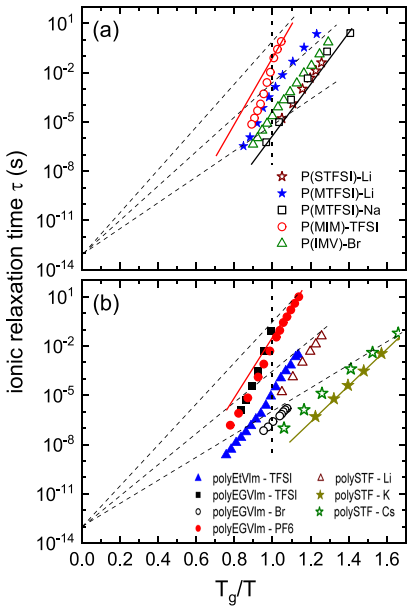

Figure 4. Characteristic times of the conductivity relaxation process as a function of T_g/T for (a) the systems investigated in this work and (b) other SICPs according to literature data.[9] The vertical dotted line corresponds to $T_g/T = 1$. In panel (a), the solid lines are examples of interpolations of sub-T_g data with eq 1 and the dashed lines are Arrhenius laws with a prefactor of 10^{-13} s, see text for details.

using a logτ axis extended down to −14 (as in Figure 3) as a function of T_g/T extended down to zero. In this way, one may directly observe that Arrhenius approximations (eq 1) indicated by the solid lines will result in the intercept values for τ_0 much smaller than 10^{-14} s. To check the generality of this observation, we included in Figure 4b the conductivity relaxation times reported in ref 9 for other SICPs. They reveal

https://doi.org/10.1021/acs.macromol.3c00879
Macromolecules 2023, 56, 6051−6059

that the classical Arrhenius description of glassy polymer data generally provides unphysically short τ_0. Note that this observation holds even for systems with large degree of decoupling, which have been experimentally explored in considerable τ and T ranges in their glassy state.

In this work, we propose another viewpoint for the temperature evolution of charge dynamics in glassy polymers, based on the broad overview provided by Figure 4. Note in this plot that the dashed lines suggests the possibility that the "true" Arrhenius behavior, with a physically reasonable prefactor of the order of 10^{-13} s, is asymptotically approached only at very low temperatures, deep in the glassy state of these materials. In other words, the activation energy barrier may not be constant, but continuously changes with temperature, even below T_g. A theoretical basis for this behavior in pure polymer glasses has been previously developed and confronted with experiments.[30] The weak evolution of the effective barrier below T_g has been predicted for polymers without ions to reflect the continuous increase of the density or a decrease in dimensionless amplitude of long wavelength density fluctuations (called S_0, which in equilibrium is the thermodynamic dimensionless isothermal compressibility) probed in small-angle scattering measurements and sometimes interpreted as the mean square fluctuation of free volume.[43] These weak changes should lead to a growth of the energy barrier with cooling even in a glassy state.[30,39]

Imposing in eq 1 a value of 10^{-13} s for τ_0, one may estimate the expected temperature evolution of the effective energy barrier for ion hopping according to

$$E^*(T) = RT\ln[\tau(T)/10^{-13}\text{s}]. \quad (3)$$

For the hereby-studied systems, the so-estimated $E^*(T)$ appears in the range 40 to 100 kJ/mol (Figure 5), significantly

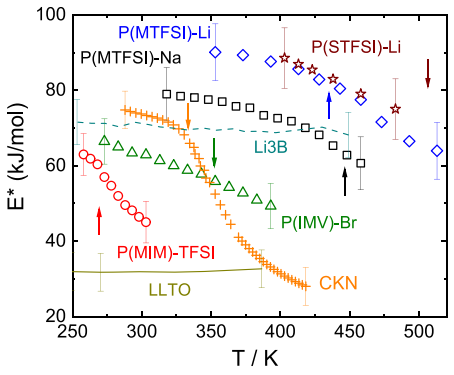

Figure 5. Effective activation energy E^* extracted for the presently investigated single ion conducting polymers (open symbols) and using literature data for CKN (crosses), Li3B (dashed line), and LLTO (solid line). The arrows indicate the corresponding glass transition temperatures. The error bars (for clarity reasons included only at the low and high limits of the investigated temperature range for each material) indicate the variation range for E^* when τ_0 changes between 10^{-12} and 10^{-14} s.

smaller than the apparent activation energy E_a (Table 1). For example, for the same material P(STFSI)-Li, the Arrhenius fit provides a constant activation energy of ~150 kJ/mol (and $\tau_0 \sim 10^{-22}$ s), while the newly proposed approach (imposing $\tau_0 = 10^{-13}$ s) suggests that this barrier is much smaller, reaching ~90 kJ/mol only at the lowest investigated temperature. Note in Figure 5 that for all polymers, E^* values change within ±10% when τ_0 is varied between 10^{-12} and 10^{-14} s.

In the same figure, we included for comparison the $E^*(T)$ estimated for the prototypical ionic melt calcium potassium nitrate (CKN).[44] As observed here and also in Figure S5 in the Supplemental Material, this material displayed behavior similar to that of conducting polymers: The temperature variation of energy barrier persists well below its calorimetric T_g (333 K). These CKN results indicate that T-dependent energy barriers may be a characteristic for a broader range of glassy conductors, not only polymers.

Figure 5 also reveals that at variance with glassy SICPs and CKN, the analysis with eq 3 provides a relatively constant $E^*(T)$ for the ionic glass Li3B and superionic ceramic LLTO. For these materials $E^*(T)$ can be identified with E_a from eq 1; hence, they may be considered to have reached the "true" Arrhenius behavior in the investigated temperature range corresponding to their deep glassy state. Based on this behavior of Li3B and LLTO one may presume that all ionic conductors will reach an Arrhenius limit with τ_0 close to 10^{-13} s at sufficiently low temperatures.

This analysis suggests that the observed unphysically short τ_0 is the consequence of the temperature variations of the energy barrier for ion hopping. Let us assume a linear T dependence of the energy barrier, $E^*(T) = E_0 - A^*RT$, at least in some limited temperature range below T_g (Figure 5). This form can be qualitatively motivated by prior theoretical work where the barrier depends on density, which grows (or S_0 decreases) roughly linearly with cooling over a sufficiently narrow range in a polymer glass.[30] Moreover, this functional form is identical to recent experimental measurements of the alpha time of vapor-deposited ultrastable polymeric glasses.[45] Then, eq 1 can be rewritten as

$$\tau = \tau_0\exp(-A)\exp(E_0/RT) \quad (4)$$

with the effective prefactor that can be much shorter than τ_0, depending on the strength of the temperature dependence of E^*. Most importantly, the apparent activation energy $E_a = E_0$ is not the real energy barrier in the given temperature range but reflects linear extrapolation of its temperature dependence to $T = 0$ K. This extrapolated value might not have any physical implication because the temperature dependence of E^* is expected to saturate at low temperatures, as will the density and S_0. The presented analysis (Figure 5, eq 4) demonstrates that the apparent Arrhenius-like temperature dependence of the relaxation time may be misleading and might provide wrong estimates of the activation energy barrier. Unphysically short values of τ_0 obtained from the Arrhenius fit (eq 1) provides a clear indication of the problem for this traditional analysis. Below, we reveal the mechanisms of the observed temperature dependence of the energy barrier for ion hopping.

Factors Controlling the Energy Barriers for Ion Hopping. The question arises if one can find any experimental evidence to confirm the temperature variations of the activation barriers for ion hopping in glassy polymers. We can safely exclude the role of segmental dynamics in these variations because in the studied systems here, the conductivity relaxation at T_g is several orders of magnitude faster than the segmental motions, *i.e.*, ion hopping occurs while structural relaxation (alpha process) is essentially frozen. As mentioned above, the Anderson–Stuart model (eq 2) suggests that the energy barrier for ion hopping is controlled by the dielectric permittivity ε and the instantaneous shear modulus G_∞. The

https://doi.org/10.1021/acs.macromol.3c00879
Macromolecules 2023, 56, 6051−6059

Coulombic interactions controlled by ε dominate the energy barrier for small ions, while the elastic forces controlled by G_∞ dominate the energy barrier for large ions.[25,29] In the following, we will consider these two limiting situations to check the impact of these parameters on the temperature dependence of the ion hopping activation barrier in glassy SICPs.

Large Mobile Ions. According to the AS model, the activation energy for relatively large ions is proportional to the instantaneous shear modulus G_∞ of the matrix; hence, our approach implies that this relationship will be preserved upon changing temperature, $E^*(T) \propto G_\infty(T)$. To check the validity of this relation, we focus on P(MIM)-TFSI and P(IMV)-Br, with the radii of mobile anions $TFSI^-$ and Br^- being 0.33 and 0.18 nm, respectively. As previously shown,[29] for $TFSI^-$, the Coulombic term in eq 2 is fairly negligible, whereas for Br^-, both elastic and Coulombic contributions are comparable. We reiterate that for testing the AS model predictions G_∞ must be determined at very high frequencies, much higher than those accessed by classical rheological techniques. For this reason, we employed Brillouin light scattering (BLS) to access the G_∞ parameter in the GHz frequency range, as described in the Methods and Analyses section.

BLS indeed revealed significant temperature dependence of G_∞ in these systems (Figure 6a,b). Moreover, direct comparison to the effective activation energy $E^*(T)$ taken from Figure 5 demonstrates that $E^*(T) \propto G_\infty(T)$ holds well for P(MIM)-TFSI in the entire studied temperature range, both above and below T_g. However, for P(IMV)-Br, an additional contribution to the energy barrier of ~30 kJ/mol. As discussed in ref 29, both elastic and Coulombic interactions are expected to provide comparable contributions to the energy barrier for hopping of this intermediate size ions. We note that in the P(IMV)-Br case, even the change in the temperature dependence of E^* occurring at T_g is also reflected in $G_\infty(T)$ results. Significant temperature variations of the shear modulus in polymers even at temperatures below T_g were reported in several earlier publications.[46−48] In comparison with ceramics and network glasses, polymers also display a significant change in density in this low temperature regime. This may result in a significant change of other parameters, including elastic constants, and consequently in a significant temperature dependence of the energy barriers for ion hopping.

Small Mobile Ions. For small ions, elastic forces become negligible and $E^*(T) \propto 1/\varepsilon(T)$ is expected (eq 2).[29] We note that it is not obvious which permittivity parameter should be used in this case of highly concentrated electrolytes. It seems reasonable to consider that for ionic rearrangements, the static permittivity (probed at frequencies lower than the ion hopping rate) might be not important, and the dielectric constant at frequencies of the conductivity relaxations or even higher should be used. Nonetheless, the permittivity spectra for P(MTFSI)-Na (Figure 7a) reveal that the overall magnitude of the dielectric strength of the conductivity process decreases upon cooling. Although for P(MTFSI)-Li, the interference of an artifact (see Methods and Analyses section) does not allow for a direct extraction of the conductivity relaxation contribution, we note that our previous works on SICPs[29] and other non-crystalline electrolytes[49−52] indicate that this anti-Curie-like behavior of dielectric strength appears to be a hallmark of the conductivity relaxation process. According to the AS model, this decrease should be qualitatively reflected in a monotonic increase in the activation energy upon cooling, as indeed observed in Figure 5 for PolyILs. Of course, such an increase could also arise to some extent from other factors such

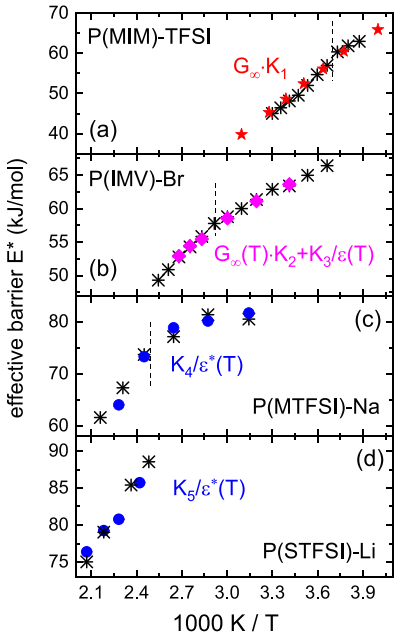

Figure 6. Temperature dependences of effective activation energies extracted for (a) P(MIM)-TFSI and (b) P(IMV)-Br are compared with those of their instantaneous shear modulus G_∞ and for (c) P(MTFSI)-Na and (d) P(STFSI)-Li with that of the inverse of permittivity ε corresponding to the characteristic frequency of ion rearrangements. To overlap the datasets, we employed the following scaling: in panel (a), G_∞ multiplied with $K_1 = 3.5 \times 10^{-8}$ kJ/(mol·Pa), in panel (b), G_∞ multiplied with $K_2 = 1.7 \times 10^{-8}$ KJ/(mol·Pa) summed with $1/\varepsilon^*(T)$ multiplied with $K_3 = 135$ kJ/mol, in panel (c), $1/\varepsilon^*(T)$ multiplied with $K_4 = 870$ kJ/mol, and in panel (d), $1/\varepsilon^*(T)$ multiplied with $K_4 = 420$ kJ/mol. The dashed vertical lines correspond to $1000/T_g$ K^{-1}.

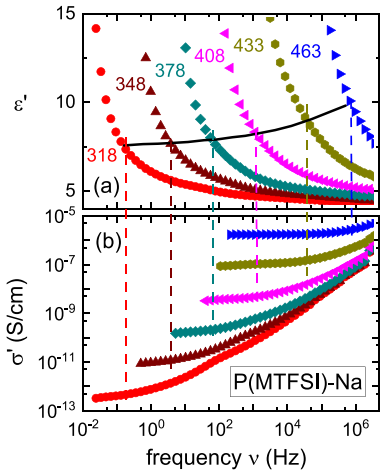

Figure 7. Frequency-dependent (a) ε' and (b) σ' responses of P(MTFSI)-Na probed at several indicated temperatures. The vertical dashed lines indicate the characteristic frequencies of conductivity relaxation processes extracted with the random barrier model (see Methods and Analyses). The black solid line corresponds to the inverse of E^* data of this material shown in Figure 5, scaled by a vertical factor. Note that the temperature dependence of $1/E^*$ matches well that of ε' values corresponding to the characteristic frequency, see text for details.

https://doi.org/10.1021/acs.macromol.3c00879
Macromolecules 2023, 56, 6051−6059

as an increase of density or decrease of S_0 in the glass, per prior theoretical analysis[24,30,37] and X-ray scattering studies.[53,54]

Figure 7a provides a comparison of the inverse of $E^*(T)$ values (black solid line) for P(MTFSI)-Na (from Figure 5), scaled by a vertical factor, with the values of $\varepsilon'(T)$. The temperature variation of $1/E^*$ appears to be in relatively good agreement with the ε' probed at the characteristic frequency of the conductivity relaxation process (indicated by the vertical dashed lines). In analogy with the instantaneous shear modulus, it appears that the dielectric constant should be taken at frequencies comparable to the rate of ion rearrangement or even higher. Therefore, we collected in Figure 6c the inverse of the permittivity value ε^* at $\nu = 1/(2\pi\tau)$ and compared its temperature dependence with that of E^* for P(MTFSI)-Na. The same procedure has been applied to P(STFSI)-Li in Figure 6d. These comparisons reveals that indeed $E^*(T) \propto 1/\varepsilon(T)$ holds well for PolyILs with small cations.

We note in Figure 7b that at the lowest investigated temperatures, the conductivity spectra signals the presence of an additional feature at frequencies between 10^1 and 10^3 Hz. This situation resembles that of other ionic conductors and is generated by the interference of secondary processes.[45,47,55] Interestingly, these relaxation features are faster than the conductivity relaxation (the latter itself being much faster than the alpha process) and hence differ from the Johari−Goldstein β-processes in the sense that they relate to the decoupled ionic motions.

The analysis presented in this section demonstrates the good applicability of the AS model to polymer electrolytes. Most important, this analysis provides strong support for the validity of the proposed picture: The activation energy of the charge transport in ion conducting polymers is not constant even deep in the glassy state because the elastic and dielectric properties (and perhaps density and S_0) of these materials continuously change with temperature even below T_g.

CONCLUSIONS

In summary, the present analysis of new and previously published data demonstrates that the traditional Arrhenius description of charge dynamics in glassy single-ion conducting polymers provides unphysically small prefactors τ_0. The newly introduced approach of imposing a value of 10^{-13} s for this parameter reveals that the effective energy barrier E^* for ion hopping is temperature-dependent even deep in the glassy state of these ion conductors. Most important, the so-estimated energy barrier appears significantly (30−40%) lower than the barrier extracted from the apparent Arrhenius dependence. Moreover, our study of the evolution of dielectric permittivity $\varepsilon(T)$ and the instantaneous shear modulus $G_\infty(T)$ provides good estimates for the evolution of $E^*(T)$ consistent with the predictions of the Anderson−Stuart model. The observed variations of the dielectric constant and instantaneous shear modulus may be partially connected with an increase in the density of these polymer glasses upon cooling.

The present analyses revealed similar behavior also in glassy CKN, suggesting that temperature dependence of the ion hopping barrier may be general not only for polymers but also for many other ion conducting glasses. This calls for a revision of many earlier data and approaches that assumed a temperature-independent activation energy for ion transport in solid-state electrolytes. In this regard, particular attention should be paid to values of τ_0. Unphysically short τ_0 ($\ll 10^{-14}$ s) might indicate the temperature-dependent energy barrier for ion hopping, and the Arrhenius analysis might significantly overestimate the latter. We stress that this approach might be applicable not only to ion transport but to many other relaxation and transport phenomena in glassy materials.

We would like to additionally emphasize that the Anderson−Stuart approach uses continuum approximations (elastic and dielectric) and microscopic discrete models are needed for a correct description of highly concentrated ionic materials. Extension of prior theoretical works for activated relaxation in pure polymer glasses[30] in conjunction with recent theory of molecular penetrant activated transport in polymer liquids[56,57] may be a promising approach in this direction.

METHODS AND ANALYSES

Differential Scanning Calorimetry. The calorimetry tests were performed using a Q1000 analyzer from TA Instruments. The samples were measured in aluminum pans with a volume of 40 μL, with a heating rate of 10 K/min. During the experiments, the flow of nitrogen was maintained at 60 mL/min. No signs of crystallization were noticed in the fully investigated temperature range. The glass transition temperatures T_g have been estimated from the recorded thermograms as the position at which the heat flow step reaches half from its melt value upon heating. The corresponding T_g values are reported in Table 1.

Dielectric Spectroscopy. The dielectric results were acquired in a 10^{-2}−10^6 Hz frequency range using an Alpha-A spectrometer from Novocontrol. The samples were placed in spacer-free dielectric cells consisting of two parallel electrode disks of 10 mm in diameter and separated by 0.2 mm. For warranting the linearity of the response, the measurements were performed using electric fields below 0.1 kV/cm. Prior to each spectrum acquisition, the temperature was stabilized within 0.1 K by a Quattro temperature controller, also from Novocontrol. The samples have been initially cooled down to 150 K and investigated upon heating. At the end of the temperature sweep, a spectrum has been remeasured near room temperature to check that the sample did not experience irreversible changes during heating.

Figures 7 and 8 present examples of dielectric spectra for P(MTFSI)-Na and P(MTFSI)-Li, respectively. Our choice was to present the dielectric response in terms of σ' and ε' representing the real parts of complex conductivity σ^* and permittivity ε^*, respectively, probed as a function of frequency ν. These two functions define the complete dielectric compliance of these materials, since σ' is directly

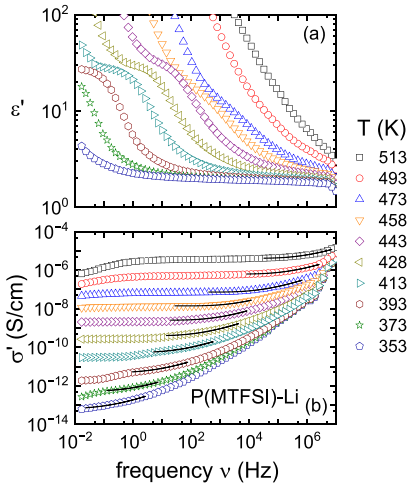

Figure 8. Frequency-dependent (a) ε' and (b) σ' responses of P(MTFSI)-Li probed at several indicated temperatures. The solid lines are predictions of the RBM according to eq 5, see text for details.

https://doi.org/10.1021/acs.macromol.3c00879
Macromolecules 2023, 56, 6051−6059

related to the dielectric loss ε'' (imaginary part of ε^*) as $\sigma' = 2\pi\nu\varepsilon_0\varepsilon''$, with ε_0 denoting the vacuum permittivity.

As observed in Figure 8a, P(MTFSI)-Li exhibits a relaxation process at low frequencies and low temperatures. Its relatively large amplitude at low T and its absence at high T indicate that this may be an artifact occurring due to the inhomogeneous filling of the dielectric cell. We note that this material has a very high T_g, above 500 K (Table 1), and it is quite possible that its lack of fluidity even at high T might have led to an incomplete filling of the cell space, especially near the edge of the bottom electrode. As can be recognized in Figure 8b, this feature occurs at frequencies lower than those characterizing the ionic relaxation (alternatively referred to as conductivity relaxation) process genuine to ionic conductors. This conductivity relaxation process marks a crossover from a "sub-diffusive" ion motion (AC-conductivity regime) governed by local ion hopping between the local minima of the energy landscape, to a regular diffusion at low frequencies (the DC-conductivity plateau).[58] The amplitude of this plateau defines the steady-state conductivity σ_0, and its frequency onset ν_0 can be interpreted as the characteristic rate with which the ions escape from their local Coulombic cage formed by neighbor counterions. One should note that in strongly decoupled materials such as P(MTFSI)-Li or any other SICP considered in this work, this relaxation process does not reflect the structural rearrangements (alpha process) of the polymer matrix, being several orders of magnitude faster than the latter.

As observed in the double-logarithmic representation of Figure 8b, a moderate cooling induces a strong decrease of both σ_0 and ν_0 parameters. At the highest investigated temperatures, the decrease in $\sigma'(\nu)$ at low frequencies is caused by the so-called electrode polarization.[59] The latter is the manifestation of the finite separation between the probing electrodes; hence, it is also not intrinsic to the investigated material.

For the parametrization of the conductivity response of the presently considered conducting polymers, we employed the refined solution of the random barrier model (RBM)

$$\ln \bar{\sigma} = i\frac{\bar{\nu}}{\bar{\sigma}}\left[1 + \frac{8}{3}i\frac{\bar{\nu}}{\bar{\sigma}}\right]^{-1/3} \tag{5}$$

connecting normalized conductivity $\bar{\sigma} \equiv \sigma^*/\sigma_0$ to the normalized frequency $\bar{\nu} \equiv \nu/\nu_0$.[60] This theoretical approach generates a $\sigma'(\nu)$ curve with a unique (material and temperature invariant) shape and relies on only two variables, σ_0 and ν_0. These can be simply extracted as the vertical and horizontal shift factors, respectively, superimposing the numerical solution of eq 5 on top of the experimental $\sigma'(\nu)$ data. As observed in Figure 8b, the RBM reproduces fairly well the spectral shape corresponding to the AC-DC crossover in $\sigma'(\nu)$.

Brillouin Light Scattering (BLS). For these investigations, P(MIM)-TFSI and P(IMV)-Br were prepared using a hot press as films, which were sandwiched between two sapphire windows. A Tandem Fabry−Perot interferometer (JRS Scientific Instruments, Table Stable Ltd) with 8 mm mirror spacing and scan amplitude of 250 nm was employed to cover a frequency range up to 8.5 GHz. Both polarized (vertical-vertical, VV) and depolarized (vertical-horizontal, VH) spectra were utilized to measure the longitudinal (L) and transverse (T) acoustic modes. The measurements were conducted using a solid-state laser (Verdi, λ_{laser} = 532 nm), in symmetric geometry at a 90° scattering angle. The power of the incident laser beam was ~0.2 mW. The samples were placed in a Janis ST-100 cryostat, with a Lakeshore controller providing a T stabilization of 0.2 K, which was achieved in about 1 h after each temperature step.

The BLS spectra recorded for P(MIM)-TFSI at temperatures varying between 250 and 323 K are included in Figure 9. Clear transversal modes (most relevant for the present context) are visible at frequencies below 3 GHz. Similar results have been obtained for P(IMV)-Br at temperatures between 293 and 373 K.

The positions of T modes in the spectra have been extracted by fit of the scattered intensities to the damped harmonic oscillator model:

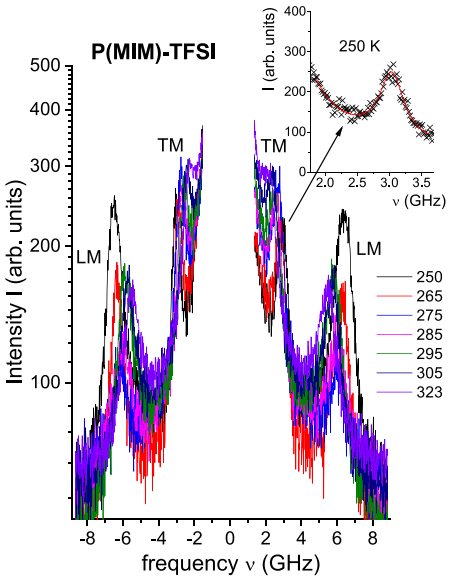

Figure 9. Light scattering spectra recorded for P(MIM)-TFSI at the temperatures indicated by numbers in Kelvin units. The inset depicts the interpolation of the spectral region including the transverse mode at 250 K using eq 6.

$$I(\omega) = \text{background} + I_0/[(\omega_{TM}^2 - \omega^2)^2 + \omega^2\gamma^2]. \tag{6}$$

Here, the first, "background" term represents the sum of a constant (as baseline) and a power law, while the second term is the relevant contribution of a damped harmonic oscillator. The latter is expressed using the amplitude I_0, the angular frequency ω_{TM} related to the characteristic frequency $\nu_{TM} = \omega_{TM}/(2\pi)$, and the damping factor γ. The inset of Figure 9 presents an example of such a fit performed for the Stokes T mode (corresponding to positive frequency shifts in the main frame) recorded at 250 K. For better statistics, at each temperature both Stokes and anti-Stokes T modes have been analyzed, and the average of the two corresponding ν_{TM} values was used in further analysis.

The advantage of symmetric scattering geometry used in our experiments is the compensation of refractive index that enables estimates of sound velocity V based on the Brillouin peak frequency ν_{TM} without the prior knowledge of the refractive index.[61] For 90° scattering

$$V = \nu_{TM}\lambda_{laser}/\sqrt{2} \tag{7}$$

In a final step, the instantaneous shear modulus G_∞ has been calculated using the relation

$$G_\infty = \rho V^2 \tag{8}$$

where ρ is the density of the material, considered in this work for both P(MIM)-TFSI and P(IMV)-Br to be 1.4 g/cm^3.

■ ASSOCIATED CONTENT

Data Availability Statement

The data that support the findings of this study are available from the corresponding authors upon reasonable request.

Supporting Information

The Supporting Information is available free of charge at https://pubs.acs.org/doi/10.1021/acs.macromol.3c00879.

Chemical details of investigated materials; calorimetric responses of investigated materials, temperature dependence of characteristic times for CKN (PDF)

https://doi.org/10.1021/acs.macromol.3c00879
Macromolecules 2023, 56, 6051−6059

AUTHOR INFORMATION

Corresponding Authors

Catalin Gainaru − *Chemical Sciences Division, Oak Ridge National Laboratory, Oak Ridge, Tennessee 37831, United States;* orcid.org/0000-0001-8295-6433; Email: gainarucp@ornl.gov

Alexei P. Sokolov − *Center for Nanophase Materials Sciences, Oak Ridge National Laboratory, Oak Ridge, Tennessee 37831, United States; Department of Chemistry, University of Tennessee, Knoxville, Tennessee 37996, United States;* orcid.org/0000-0002-8187-9445; Email: sokolov@utk.edu

Authors

Rajeev Kumar − *Center for Nanophase Materials Sciences, Oak Ridge National Laboratory, Oak Ridge, Tennessee 37831, United States;* orcid.org/0000-0001-9494-3488

Ivan Popov − *Department of Chemistry, University of Tennessee, Knoxville, Tennessee 37996, United States;* orcid.org/0000-0002-7235-2043

Md Anisur Rahman − *Chemical Sciences Division, Oak Ridge National Laboratory, Oak Ridge, Tennessee 37831, United States;* orcid.org/0000-0002-7190-9751

Michelle Lehmann − *Chemical Sciences Division, Oak Ridge National Laboratory, Oak Ridge, Tennessee 37831, United States*

Eric Stacy − *Department of Chemistry, University of Tennessee, Knoxville, Tennessee 37996, United States*

Vera Bocharova − *Chemical Sciences Division, Oak Ridge National Laboratory, Oak Ridge, Tennessee 37831, United States;* orcid.org/0000-0003-4270-3866

Bobby G. Sumpter − *Center for Nanophase Materials Sciences, Oak Ridge National Laboratory, Oak Ridge, Tennessee 37831, United States;* orcid.org/0000-0001-6341-0355

Tomonori Saito − *Chemical Sciences Division, Oak Ridge National Laboratory, Oak Ridge, Tennessee 37831, United States;* orcid.org/0000-0002-4536-7530

Kenneth S. Schweizer − *Departments of Materials Science and Chemistry, University of Illinois, Urbana, Illinois 61801, United States*

Complete contact information is available at: https://pubs.acs.org/10.1021/acs.macromol.3c00879

Notes

The authors declare no competing financial interest.

ACKNOWLEDGMENTS

This work was supported as part of the Fast and Cooperative Ion Transport in Polymer-Based Materials (FaCT), an Energy Frontier Research Center funded by the U.S. Department of Energy, Office of Science, Basic Energy Sciences at Oak Ridge National Laboratory and University of Illinois Urbana-Champaign under contract DE-AC05-00OR22725. I.P. thanks NSF (award CHE-2102425) for partial financial support of the BLS measurements. BGS acknowledges support from the Center for Nanophase Materials Sciences, a US Department of Energy Office of Science User Facility at Oak Ridge National Laboratory.

REFERENCES

(1) Li, Y.; Wang, X.; Dong, S.; Chen, X.; Cui, G. Recent Advances in Non-Aqueous Electrolyte for Rechargeable Li-O2 Batteries. *Adv. Energy Mater.* **2016**, *6*, 1600751.

(2) Manthiram, A.; Yu, X.; Wang, S. Lithium Battery Chemistries Enabled by Solid-State Electrolytes. *Nat. Rev. Mater.* **2017**, *2*, 16103.

(3) Bachman, J. C.; Muy, S.; Grimaud, A.; Chang, H. H.; Pour, N.; Lux, S. F.; Paschos, O.; Maglia, F.; Lupart, S.; Lamp, P.; Giordano, L.; Shao-Horn, Y. Inorganic Solid-State Electrolytes for Lithium Batteries: Mechanisms and Properties Governing Ion Conduction. *Chem. Rev.* **2016**, *116*, 140.

(4) Osada, I.; de Vries, H.; Scrosati, B.; Passerini, S. Ionic-Liquid-Based Polymer Electrolytes for Battery Applications. *Angew. Chem., Int. Ed.* **2016**, *55*, 500.

(5) Muldoon, J.; Bucur, C. B.; Boaretto, N.; Gregory, T.; di Noto, V. Polymers: Opening Doors to Future Batteries. *Polym. Rev.* **2015**, *55*, 208.

(6) Yi, J.; Guo, S.; He, P.; Zhou, H. Status and Prospects of Polymer Electrolytes for Solid-State Li−O2 (Air) Batteries. *Energy Environ. Sci.* **2017**, *10*, 860.

(7) Hu, P.; Chai, J.; Duan, Y.; Liu, Z.; Cui, G.; Chen, L. Progress in Nitrile-Based Polymer Electrolytes for High Performance Lithium Batteries. *J. Mater. Chem. A* **2016**, *4*, 10070.

(8) Kato, Y.; Hori, S.; Saito, T.; Suzuki, K.; Hirayama, M.; Mitsui, A.; Yonemura, M.; Iba, H.; Kanno, R. High-Power All-Solid-State Batteries Using Sulfide Superionic Conductors. *Nat. Energy* **2016**, *1*, 16030.

(9) Stacy, E. W.; Gainaru, C. P.; Gobet, M.; Wojnarowska, Z.; Bocharova, V.; Greenbaum, S. G.; Sokolov, A. P. Fundamental Limitations of Ionic Conductivity in Polymerized Ionic Liquids. *Macromolecules* **2018**, *51*, 8637−8645.

(10) Angell, C. A. Fast ion motion in glassy and amorphous materials. *Solid State Ionics* **1983**, *9-10*, 3−16.

(11) Ratner, M. A.; Shriver, D. F. Ion transport in solvent-free polymers. *Chem. Rev.* **1988**, *88*, 109−124.

(12) Bocharova, V.; Sokolov, A. P. Perspectives for Polymer Electrolytes: A View from Fundamentals of Ionic Conductivity. *Macromolecules* **2020**, *53*, 4141−4157.

(13) Edman, L.; Doeff, M. M.; Ferry, A.; Kerr, J.; De Jonghe, L. C. Transport Properties of the Solid Polymer Electrolyte System $P(EO)_nLiTFSI$. *J. Phys. Chem. B* **2000**, *104*, 3476−3480.

(14) Mecerreyes, D. Polymeric ionic liquids: Broadening the properties and applications of Polyelectrolytes. *Prog. Polym. Sci.* **2011**, *36*, 1629.

(15) Nishimura, N.; Ohno, H. 15th anniversary of polymerised ionic liquids. *Polymer* **2014**, *55*, 3289.

(16) Yuan, J.; Mecerreyes, D.; Antonietti, M. Poly(ionic liquid)s: an update. *Prog. Polym. Sci.* **2013**, *38*, 1009.

(17) Eftekhari, A.; Saito, T. Synthesis and properties of polymerized ionic liquids. *Eur. Polym. J.* **2017**, *90*, 245.

(18) Gainaru, C.; Stacy, E. W.; Bocharova, V.; Gobet, M.; Holt, A. P.; Saito, T.; Greenbaum, S.; Sokolov, A. P. Mechanism of conductivity relaxation in liquid and polymeric electrolytes: Direct link between conductivity and diffusivity. *J. Phys. Chem. B* **2016**, *120*, 11074.

(19) Choi, U. H.; Ye, Y.; Salas de la Cruz, D.; Liu, W.; Winey, K. I.; Elabd, Y. A.; Runt, J.; Colby, R. H. Dielectric and Viscoelastic Responses of Imidazolium-Based Ionomers with Different Counter-ions and Side Chain Lengths. *Macromolecules* **2014**, *47*, 777−790.

(20) Bocharova, V.; Wojnarowska, Z.; Cao, P.-F.; Fu, Y.; Kumar, R.; Li, B.; Novikov, V. N.; Zhao, S.; Kisliuk, A.; Saito, T.; Mays, J. W.; Sumpter, B. G.; Sokolov, A. P. Influence of Chain Rigidity and Dielectric Constant on the Glass Transition Temperature in Polymerized Ionic Liquids. *J. Phys. Chem. B* **2017**, *121*, 11511−11519.

(21) Fan, F.; Wang, W.; Holt, A. P.; Feng, H.; Uhrig, D.; Lu, X.; Hong, T.; Wang, Y.; Kang, N.-G.; Mays, J.; Sokolov, A. P. Effect of molecular weight on the ion transport mechanism in polymerized ionic liquids. *Macromolecules* **2016**, *49*, 4557.

(22) Mizuno, F.; Belieres, J. P.; Kuwata, N.; Pradel, A.; Ribes, M.; Angell, C. A. Highly decoupled ionic and protonic solid electrolyte systems, in relation to other relaxing systems and their energy landscapes. *J. Non-Cryst. Solids* **2006**, *352*, 5147−5155.
(23) Ingram, M. D. Ionic conductivity and glass structure. *Philos. Mag. B* **1989**, *60*, 729−740.
(24) Dyre, J. C.; Christensen, T. E.; Olsen, N. B. Elastic models for the non-Arrhenius viscosity of glass-forming liquids. *J. Non-Cryst. Solids* **2006**, *352*, 4635−4642.
(25) Mirigian, S.; Schweizer, K. S. Elastically cooperative activated barrier hopping theory of relaxation in viscous fluids. II. Thermal liquids. *J. Chem. Phys.* **2014**, *140*, 194507.
(26) Mirigian, S.; Schweizer, K. S. Dynamical Theory of Segmental Relaxation and Emergent Elasticity in Supercooled Polymer Melts. *Macromolecules* **2015**, *48*, 1901.
(27) Ngai, K. L., *Relaxation and Diffusion in Complex Systems* (Springer, New York, 2011).
(28) Anderson, O. L.; Stuart, D. A. Calculation of activation energy of ionic conductivity in silica glasses by classical methods. *J. Am. Ceramic Soc.* **1954**, *37*, 573−580.
(29) Dyre, J. C. Colloquium: The glass transition and elastic models of glass-forming liquids. *Rev. Mod. Phys.* **2006**, *78*, 953−972.
(30) Hecksher, T.; Dyre, J. C. A review of experiments testing the shoving model. *J. Non-Cryst. Solids* **2015**, *407*, 14−22.
(31) McElfresh, D. K.; Howitt, D. G. A structure based model for diffusion in glass and the determination of diffusion constants in silica. *J. Non-Cryst. Solids* **1990**, *124*, 174−180.
(32) Kisliuk, A.; Bocharova, V.; Popov, I.; Gainaru, C.; Sokolov, A. P. Fundamental parameters governing ion conductivity in polymer electrolytes. *Electrochim. Acta* **2019**, *299*, 191−196.
(33) Chen, K.; Schweizer, K. S. Theory of relaxation and elasticity in polymer glasses. *J. Chem. Phys.* **2007**, *126*, 014904−014910.
(34) Dyre, J. C.; Maass, P.; Roling, B.; Sidebottom, D. L. Fundamental questions relating to ion conduction in disordered solids. *Rep. Prog. Phys.* **2009**, *72*, No. 046501.
(35) Habasaki, J.; León, C.; Ngai, K. L. *Dynamics of Glassy, Crystalline and Liquid Ionic Conductors: Experiments, Theories, Simulations;* Springer, Switzerland, 2017
(36) Sangoro, J. R.; Iacob, C.; Agapov, A. L.; Wang, Y.; Berdzinski, S.; Rexhausen, H.; Strehmel, V.; Friedrich, C.; Sokolov, A. P.; Kremer, F. Decoupling of ionic conductivity from structural dynamics in polymerized ionic liquids. *Soft Matter* **2014**, *10*, 3536.
(37) Kumar, B.; Koka, S.; Rodrigues, S. J.; Nookala, M. Physical aging effects on conductivity in polymer electrolytes. *Solid State Ionics* **2003**, *156*, 163−170.
(38) Paluch, M.; Wojnarowska, Z.; Hensel-Bielowka, S. Heterogeneous Dynamics of Prototypical Ionic Glass CKN Monitored by Physical Aging. *Phys. Rev. Lett.* **2013**, *110*, No. 015702.
(39) Dyre, J. C. Aging of CKN: Modulus Versus Conductivity Analysis. *Phys. Rev. Lett.* **2013**, *110*, No. 245901.
(40) Rivera-Calzada, A.; Santamaría, J.; Blochowicz, T.; Gainaru, C.; Rössler, E. A.; Leon, C. *Unpublished Data*.
(41) Chen, K.; Schweizer, K. S. Microscopic constitutive equation theory for the nonlinear mechanical response of polymer glasses. *Macromolecules* **2008**, *41*, 5908.
(42) McKenna, G. B.; Simon, S. L. 50th Anniversary Perspective: Challenges in the Dynamics and Kinetics of Glass-Forming Polymers. *Macromolecules* **2017**, *50*, 6333−6361.
(43) Roe, R. J. Density fluctuation in a "Theorist's ideal glass,". *J. Chem. Phys.* **1983**, *79*, 936.
(44) Pimenov, A.; Loidl, A.; Böhmer, R. Structural relaxation in a molten salt probed by time-dependent dc conductivity measurements. *J. Non-Cryst. Solids* **1997**, *212*, 89−94.
(45) Kong, D.; Meng, Y.; McKenna, G. B. Searching for the ideal glass transition: Going to yotta seconds and beyond. *J. Non-crystalline Solids* **2023**, *606*, No. 122186.
(46) Xu, B.; McKenna, G. B. Evaluation of the Dyre shoving model using dynamic data near the glass temperature. *J. Chem. Phys.* **2011**, *134*, 124902.
(47) Kleiber, C.; Hecksher, T.; Pezeril, T.; Torchinsky, D. H.; Dyre, J. C.; Nelson, K. A. Mechanical spectra of glass-forming liquids. II. Gigahertz-frequency longitudinal and shear acoustic dynamics in glycerol and DC704 studied by time-domain Brillouin scattering. *J. Chem. Phys.* **2013**, *138*, 12A544.
(48) Mulliken, A. D.; Boyce, M. C. Mechanics of the rate-dependent elastic−plastic deformation of glassy polymers from low to high strain rates. *Int. J. Solids Struct.* **2006**, *43*, 1331.
(49) Wieland, F.; Bocharova, V.; Münzner, P.; Hiller, W.; Sakrowski, R.; Sternemann, C.; Böhmer, R.; Sokolov, A. P.; Gainaru, C. Structure and dynamics of short-chain polymerized ionic liquids. *J. Chem. Phys.* **2019**, *151*, No. 034903.
(50) Münzner, P.; Hoffmann, L.; Böhmer, R.; Gainaru, C. Deeply supercooled aqueous LiCl solution studied by frequency-resolved shear rheology. *J. Chem. Phys.* **2019**, *150*, No. 234505.
(51) Thomann, C. A.; Münzner, P.; Moch, K.; Jacquemin, J.; Goodrich, P.; Sokolov, A. P.; Böhmer, R.; Gainaru, C. Tuning the dynamics of imidazolium-based ionic liquids via hydrogen bonding. I. The viscous regime. *J. Chem. Phys.* **2020**, *153*, 194501.
(52) Ahlmann, S.; Münzner, P.; Moch, K.; Sokolov, A. P.; Böhmer, R.; Gainaru, C. The relationship between charge and molecular dynamics in viscous acid hydrates. *J. Chem. Phys.* **2021**, *155*, No. 014505.
(53) Roe, R. J.; Curro, J. J. Small-angle x-ray scattering study of density fluctuation in polystyrene annealed below the glass transition temperature. *Macromolecules* **1983**, *16*, 428.
(54) Tanabe, Y.; Muller, N.; Fischer, E. W. Density Fluctuation in Amorphous Polymers by Small Angle X-Ray Scattering. *Polymer J.* **1984**, *16*, 445.
(55) Wojnarowska, Z.; Musiał, M.; Cheng, S.; Drockenmuller, E.; Paluch, M. Fast secondary dynamics for enhanced charge transport in polymerized ionic liquids Phys. *Rev. E* **2020**, *101*, No. 032606.
(56) Mei, B.; Schweizer, K. S. Activated penetrant dynamics in glass forming liquids: size effects, decoupling, slaving, collective elasticity and correlation with matrix compressibility. *Soft Matter* **2021**, *17*, 2624−2639.
(57) Mei, B.; Sheridan, G. S.; Evans, C. M.; Schweizer, K. S. Elucidation of the physical factors that control activated transport of penetrants in chemically complex glass-forming liquids. *PNAS.* **2022**, *119*, No. e2210094119.
(58) Sidebottom, D. L. Colloquium: Understanding ion motion in disordered solids from impedance spectroscopy scaling. *Rev. Mod. Phys.* **2009**, *81*, 999.
(59) Ben Ishai, P.; Talary, M. S.; Caduff, A.; Levy, E.; Feldman, Y. Electrode polarization in dielectric measurements: a review. *Meas. Sci. Technol.* **2013**, *24*, No. 102001.
(60) The presently employed solution of the Random Barrier Model is provided as Supplemental Material in Schrøder, T. B.; Dyre, J. C. ac Hopping Conduction at Extreme Disorder Takes Place on the Percolating Cluster. *Phys. Rev. Lett.* **2008**, *101*, No. 025901.
(61) Krüger, J. K.; Embs, J.; Brierley, J.; Jiménez, R. A new Brillouin scattering technique for the investigation of acoustic and opto-acoustic properties: Application to polymers. *J. Phys. D: Appl. Phys.* **1998**, *31*, 1913−1917.

https://doi.org/10.1021/acs.macromol.3c00879
Macromolecules 2023, 56, 6051−6059